ORIGINAL PAPER

Relationship between mutation of serine residue at 315th position in *M. tuberculosis* catalase-peroxidase enzyme and Isoniazid susceptibility: An in silico analysis

Rituraj Purohit · Vidya Rajendran ·
Rao Sethumadhavan

Abstract Remarkable advances have been made in the drug therapy of tuberculosis. However much remains to be learned about the molecular and structural basis of drug resistance in *Mycobacterium tuberculosis*. It is known that, activation of Isoniazid (INH) is mediated by *Mycobacterium tuberculosis* catalase-peroxidase (*MtB*KatG) and mutation at position 315 (serine to threonine) leads to resistance. We have conducted studies on the drug resistance through docking and binding analysis supported by time-scale (~1000 ps) and unrestrained all-atom molecular dynamics simulations of wild and mutant *MtB*KatG. The study showed conformational changes of binding residues. Mutant (S315T) showed high docking score and INH binding affinity as compared to wild enzyme. In molecular dynamics simulation, mutant enzyme exhibited less structure fluctuation at INH binding residues and more degree of fluctuation at C-terminal domain compared to wild enzyme. Our computational studies and data endorse that *MtB*KatG mutation (S315T) decrease the flexibility of binding residues and made them rigid by altering the conformational changes, in turn it hampers the INH activity. We ascertain from this work that, this study on structural mechanism of resistance development in *Mycobacterium tuberculosis* would lead to new therapeutics based on the result obtained in this study.

Keywords Binding affinity · Catalase-peroxidase · Docking · Isoniazid · Molecular dynamic simulation · Resistance mutation · Solvent accessibility

R. Purohit · V. Rajendran · R. Sethumadhavan (✉)
School of Bio Sciences and Technology (SBST), Bioinformatics
Division, Vellore Institute of Technology University,
Vellore 632014, Tamil Nadu, India
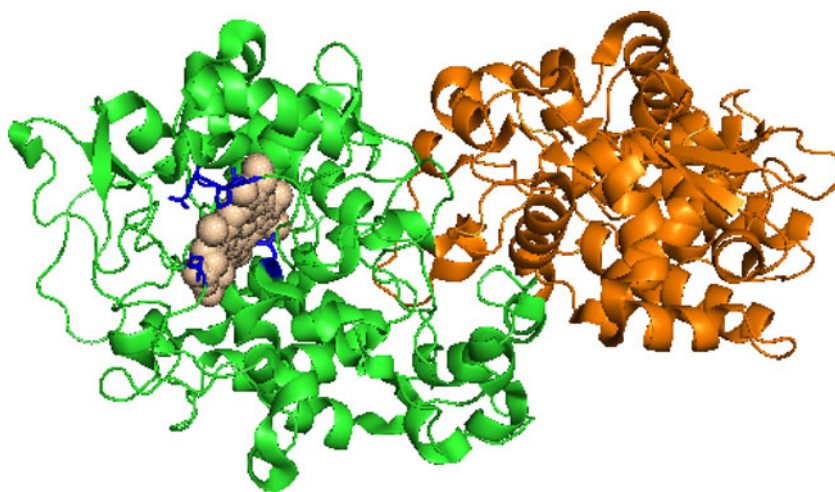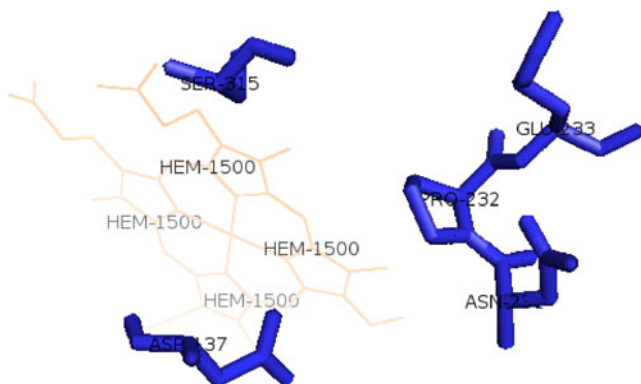e-mail: rsethumadhavan@vit.ac.in

Introduction

Mycobacterium tuberculosis Catalase-peroxidase (*MtB*KatG) enzyme has evolved by gene duplication from an ancestral peroxidase. They are multimeric heme enzymes with 80–81-kDa subunits having high sequence homology in their N-terminal halves to cytochrome *c* peroxidase and ascorbate peroxidase, especially in the distal and proximal heme regions [1].

*MtB*KatG is important for the virulence of the pathogen *Mycobacterium,* because of its role in the removal of peroxide in infected host macrophage [2]. This enzyme exhibits both high catalase activity and a broad spectrum peroxidase activity for which a physiologically relevant substrate has not been identified [3, 4].

*MtB*KatG is also responsible for activation of Isoniazid (INH) a *pro*-drug, which has been in continual use since the early 1950s to treat tuberculosis infection [4–6]. In vitro, INH is oxidized by *MtB*KatG [7, 8] to an acylating species, most likely an acyl radical, that forms an isonicotinoyl-nicotinamide adenine dinucleotide adduct (IN-NAD) when it reacts with NAD [9]. In most cases *Mycobacterium* becomes resistances to INH. It has been proved that resistance is due to some mutations in *MtB*KatG enzyme. The most common INH resistance mutations in *Mycobacterium tuberculosis* clinical isolates occur in *MtB*KatG [10], and replacements at residue Ser315 are the most commonly encountered in the mutated *MtB*KatG gene of INH-resistant strains [11, 12]. Mutant S315T, confers high level drug resistance (up to a 200-fold increase in minimum inhibitory concentration (MIC) that kills 50% of bacteria is the most frequent and is found in more than 50% of INH-resistant isolates of *Mycobacterium tuberculosis* [13, 14]. In vitro, this mutant enzyme exhibits a very poor rate of peroxidation/activation of the antibiotic, although the enzyme has

Fig. 1 Monomer structure of native *Mtb*KatG enzyme (1SJ2). The N-terminal domain is shown in *green*, and C-terminal domain is shown in *orange*, binding residues (137D, 230 V, 231 N, 232P and 315 S) are shown in *blue* stick model and the heme is shown in spheres model

close to normal catalase activity and peroxidase activity w7ith substrates other than INH [15, 16]. Thus, replacements at residue 315th position of *Mtb*KatG are expected to interfere with drug binding and activation in general as for *Mtb*KatG(S315T), without broadly compromising heme structure and function [17]. The *Mtb*KatG(S315T) mutant is generally interesting because enzyme functions are preserved despite the poor interaction with INH, thereby preserving bacterial physiology and virulence [18]. Three dimension structural insights into the mechanism of Isoniazid resistance can also be gained from the study of naturally occurring *Mtb*KatG mutant.

We analyzed one *Mtb*KatG monomer which contains N-terminal and C-terminal domain, shown in Fig. 1. Both domains are important for functional activity of enzyme but INH and heme binding site present only in N-terminal domain N_{1-440}, that when modified affect enzyme activity. In *Mtb*KatG, INH binding residues includes 137D, 230 V, 231 N, 232P and 315 S [19], INH binding pocket shown in Fig. 2. On the other hand C-terminal domain $C_{420-744}$ has less sequence similarity, and does not have the conserved

heme active-site motif characteristic of peroxidases but deletion of C-terminal domain results in inactive enzyme [3, 20].

The main goal in this work is to examine the structural behavior of wild and mutant *Mtb*KatG(S315T) and to comprehend the resistant nature of the mutant enzyme. We report docking, binding and structural analysis of INH binding residues in wild and mutant *Mtb*KatG enzyme. We also incorporate the explicit molecular dynamics simulation analysis in water to understand changes in structural behavior with time evolution.

Materials and methods

Datasets

We selected one wild type *Mtb*KatG 1SJ2 [19] and a mutant type (S315T) 2CCD [21] structure from Brookhaven Protein Data Bank [22]. One small molecule/inhibitor, Isoniazid was chosen for our investigation. Both these structures were solved with >2.0 Å resolution. The SMILES strings were collected from PubChem, a database maintained in NCBI [23], and submitted to CORINA (www.molecular-networks.com/online_demos/corina_demo.html) for constructing the 3D structure of small molecule. Our study is based on in silico analysis, so we did not go for any ethical approval.

Computation of docking score and interaction energy between the inhibitor and *Mtb*KatG enzyme

The web server PatchDock [24] was used to compute the scores of docked complexes. 3D coordinates of all the individual receptor and the inhibitor were submitted in PDB format with default parameters. The region near the δ-*meso* edge of the heme is suggested to be the most favoured site

Fig. 2 INH Binding pocket of native *Mtb*KatG enzyme (1SJ2). Binding residues (137D, 230 V, 231 N, 232P and 315 S) are shown in *blue* stick model and the heme is shown in *wheat* line model

Table 1 Docking score and ligand–receptor interaction energies of *MtB*KatG wild and mutant complex with INH

PDB ID	Docking sore	Ligand-receptor electrostatic energy (kcal/mol)	Ligand-receptor van der Waals energy (kcal/mol)	Total ligand-receptor interaction energy (kcal/mol)
1SJ2 (wild)	2640	-0.19	-3.23	-3.86
2CCD (mutantS315T)	2874	-0.76	-6.32	-7.53

for INH binding in *MtB*KatG [18] and hence, binding site residues 137D, 230 V, 231 N, 232P and 315 S/T of *MtB*KatG were given as one of the additional input to the server. The underlying principle of this server is based on molecular shape representation, surface patch matching plus filtering and scoring.

The interaction energy of the complex was calculated by PEARLS web server [25]. The server computed total ligand-receptor interaction energy and its components are computed by an atomic level molecular mechanics-based force field involving intermolecular van der Waals, electrostatic and hydrogen bond interactions between the binding molecule and its receptor. The electrostatic energy is particularly well suited for analyzing recognition process because it is a physically meaningful representation of how a molecule is perceived by another molecule in its vicinity. The negative value of electrostatic energy enables better interaction and vice-versa. The proper formation of hydrogen bonds and van der Waals contacts require complementarity of the surfaces involved. Such surfaces must be able to pack closely together, creating many contact points, and charged atoms must be properly positioned to make electrostatic bonds. Thus van der Waals and polar interactions contribute to the dynamic stability of the ligand-receptor complex [26].

Individual monomer the receptor and the ligand molecule were given as input for performing the docking experiments. Default root-mean-square deviation (RMSD) value (4.00 Å) was used and we were given the receptor binding site residues information docking experiments. It generated several complex structures based on docking scores. The complex structure file, with the best docking score was given as input to PEARLS to perform the interaction analysis.

Structural and functional analysis of INH binding residue by computing solvent accessibility

Solvent accessibility is the ratio between the solvent accessible surface area of a residue in three-dimensional structures and that in an extended tripeptide conformation [27]. It indicates the packing arrangement of residues. The solvent accessible surface area is defined as the locus of the center of the solvent molecule as it rolls over the van der Waals surface of the protein. It is typically calculated using the 'rolling ball' algorithm [28].

We obtained the solvent accessibility information by using WHAT IF web server [29]. We have analyzed for both wild and mutant enzyme and estimated the solvent accessibility of INH binding residues.

Molecular dynamics simulation

Molecular dynamics simulations were performed using the GROMACS 4.0.5 [30, 31] running on a single 2.8 GHz Pentium IV IBM machine with 512 MB RAM and running Fedora Core 2 Linux package and GROMOS96 [32] 43a1 force field implemented on LINUX architecture. Monomer of crystal structure of wild (1SJ2) [19] and mutant (2CCD) *MtB*KatG [21] were used as the starting point for MD simulations. Crystallographic waters and were not included. The protein was solvated in a cubic 0.9 nm of 15960 SPC [33] water molecules. The simulation system was set up as an NPT ensemble, i.e., constant number of particles (N), constant pressure (P) and constant temperature (T). All protein atoms were at a distance equal to 1.0 nm from the box edges. The system was subjected to energy minimization for 1000 steps by steepest descent. The minimized system was equilibrated for 100 picoseconds (ps) each at 300 K by position restrained molecular dynamics simulation. The equilibrated systems were then subjected to molecular dynamics simulations for 1000 ps each at 300 K. In all simulations, the temperature was kept constant at 300 K with a Berendsen thermostat [34]. The particle mesh Ewald method [35] was used to treat long-range Coulombic interactions and the simulations performed using the SANDER module [36]. The ionization states of the residues were set appropriate to pH 7 with all histidines

Table 2 Solvent accessibility analysis at INH binding residues *MtB*KatG of wild and mutant enzyme

PDB ID	Solvent accessibility at INH binding residues (in Å)				
	D137	V230	N231	P232	S/T315
1SJ2 (wild)	9.14	1.4	7.9	6.9	13.1
2CCD (mutantS315T)	3.9	2.0	6.5	4.5	12.0

Table 3 C-alpha carbon root mean square mean fluctuation (in nm) of binding residues of *MtB*KatG wild and mutant enzyme

PDB ID	RMSF of C-alpha carbon at INH binding residues (in nm)				
	D137	V230	N231	P232	S/T315
1SJ2 (wild)	0.044	0.047	0.052	0.064	0.073
2CCD (mutantS315T)	0.039	0.028	0.051	0.051	0.060

assumed to be neutral. The SHAKE algorithm was used to constrain bond lengths involving hydrogen, permitting a time step of 2 femtoseconds. Van der Waals and coulomb interactions were truncated at 1.0 nm. The non-bonded pair list was updated every 10 steps and conformations were stored every 0.5 ps. Other analyses were performed using scripts included with the Gromacs [30] distribution.

The trajectory files were analyzed through the use of g_rms and g_rmsf GROMACS utilities in order to obtain the RMSD and the RMSF (root-mean-square fluctuation) values. The number of distinct hydrogen bonds within the enzyme and hydrogen bonds of binding residues to other amino acids within the protein during the simulation (*N*Hbond) were calculated using g_hbond. *N*Hbond determined on the basis of donor–acceptor distance smaller than 0.35 nm and of donor–hydrogen-acceptor angle larger than 150°. Moreover VMD [37] and Coot [38] packages were used for trajectory analysis and for the management of the simulation snapshot structures. The major focus of this study was to compare the dynamic behaviors of wild and mutant enzyme at 300 K. To that end we compared the RMSF of C-alpha carbon and RMSD of backbone structure of protein between the trajectories generated at 300 K to investigate the flexible nature of mutant. In order to plot RMSD and RMSF of the three dimensional backbone of C-alpha carbon and motion projection of the protein in phase space of the system, we used ORIGIN program (version 6.0).

Results and discussion

An understanding of the molecular basis of action of existing agents such as Isoniazid would provide a useful foundation for new drug development. The goal of this work is to understand the three dimensional spatial arrangement and conformational changes due to mutation at important residues participating in INH binding.

Docking score illustrate the extent of interactions of a ligand with the receptor. Our docking analysis shows the behavior of protein–ligand complex of *MtB*KatG enzyme with INH. The docking score of wild enzyme-INH complex and mutant enzyme-INH complex are found to be 2640 and 2874 respectively (Table 1). Calculation of interaction energy is very important to understand the biological activity of most ligand molecules. Overall interaction energy of the complex mostly contributed to van der Waals and electrostatic interaction energy between *MtB*KatG (wild and mutant) and INH. Estimates of van der Waals interaction energy was computed to provide a theoretical quantitative assessment of the enzyme-ligand non-bonded interactions. In the wild complex, the van der Waals energy was -3.23 kcal mol^{-1} and electrostatic energy was -0.19 kcal mol^{-1}. The total ligand receptor interaction energy of wild and mutant *MtB*KatG complex is found to be -3.86 and -7.53 kcal mol^{-1} respectively. The total interaction energy of the mutant complex contributed more by van der

Fig. 3 Time evolution of backbone RMSDs are shown as a function of time of wild and mutant structures at 300 K. The symbol coding scheme is as follows: wild (solid line) and mutant (dashed line)
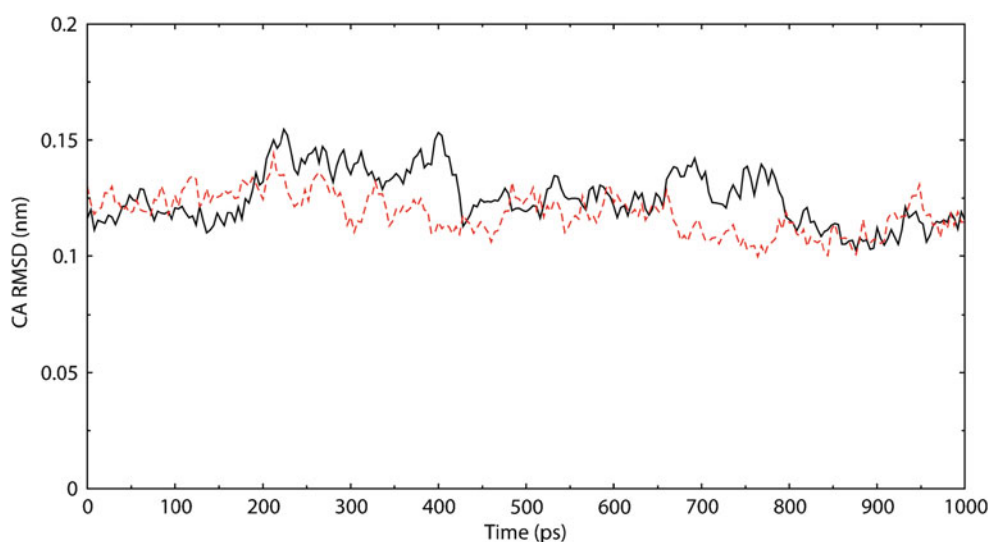
Fig. 4 Root-mean-square fluctuations of the backbone C-alpha carbon of all residues over the entire simulation. The symbol coding scheme is as follows: wild (solid lines) and mutant (dotted lines)
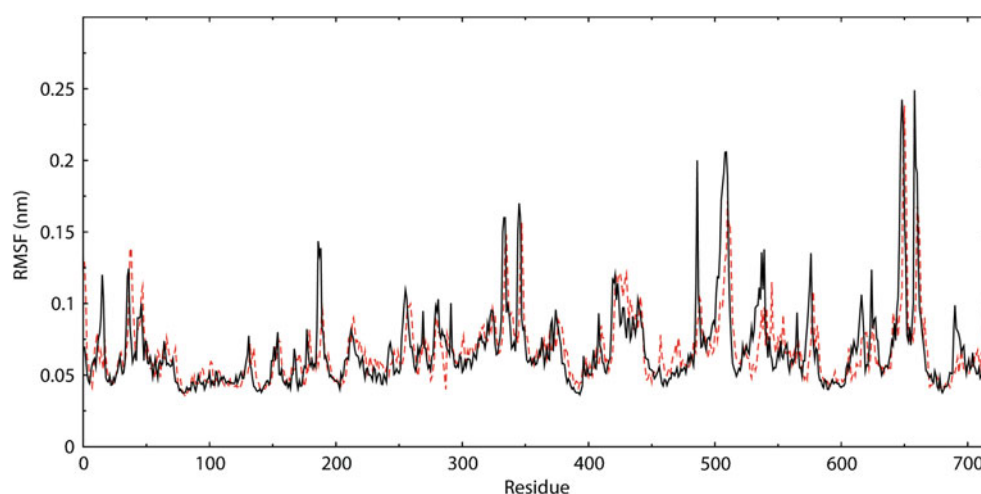
Waals energy and has the value -6.32 kcal mol^{-1} (Table 1). High docking score and lower energy of the mutant complex indicates tight binding between mutant *MtB*KatG and INH. Due to this strong binding, INH is unable to convert itself into active form (IN-NAD), which is important for its lethal activity and remains unsusceptible toward mutant *MtB*KatG. The two factors, namely, score difference in docking process and variation in binding energy of the complex probably corresponds to conformational alteration of binding residues.

In above analysis, mutant shows more ligand interaction and docking score compared to wild enzyme which inspired us to investigate the structural arrangement of biding residues in 3D space. Solvent accessibility of amino acids involved in structural and functional role of wild and mutant of *MtB*KatG is also analyzed. Compared to mutant, wild enzyme showed higher solvent accessibility at binding residues (Table 2). It indicates the occupancy of drug molecule at binding
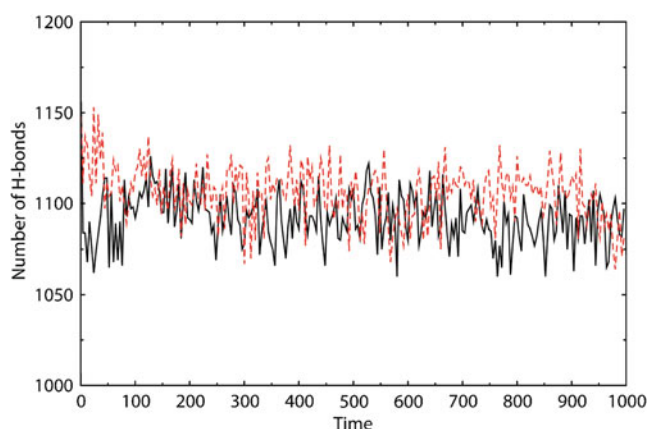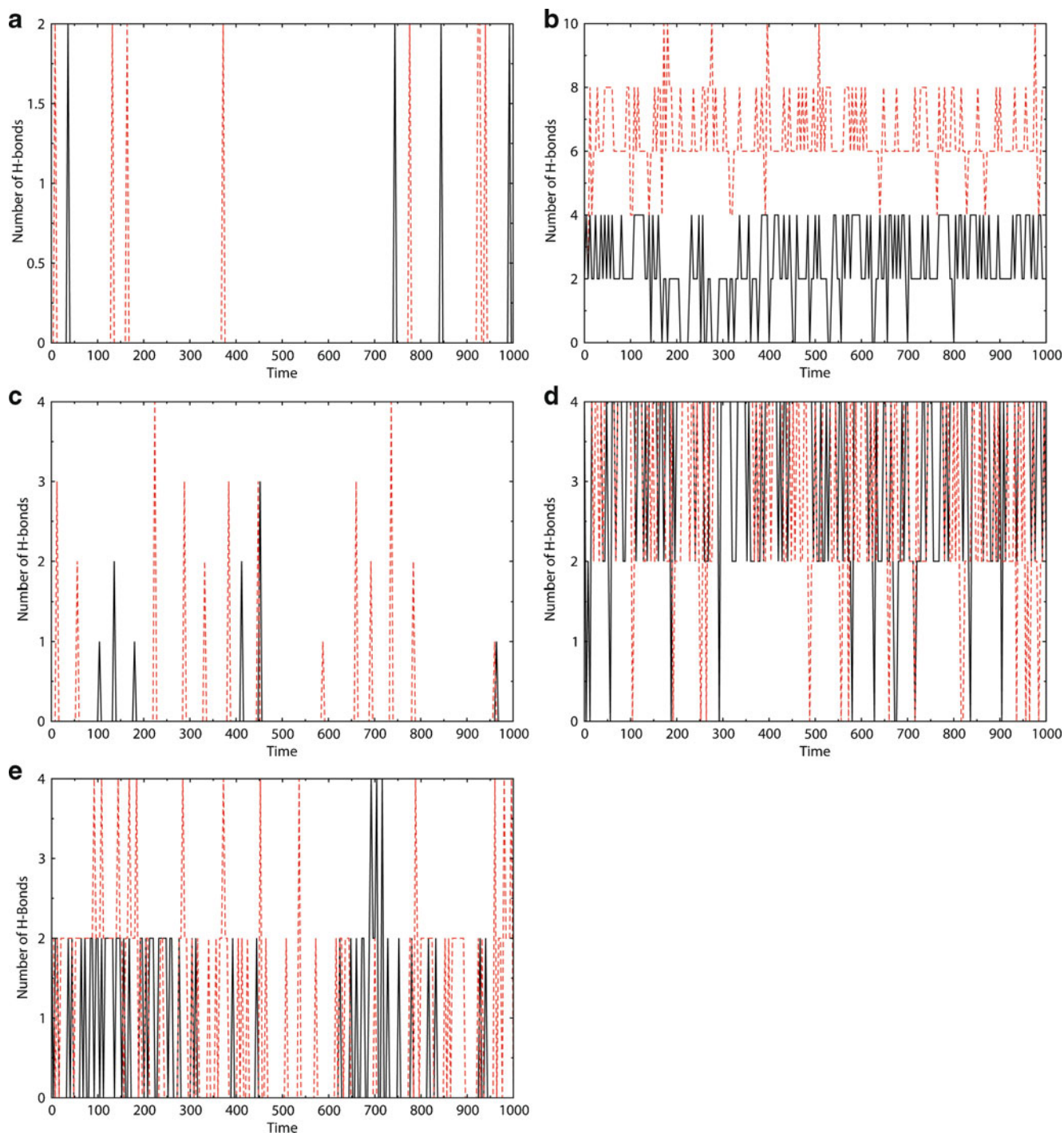
site. Binding residues of wild enzyme located at exposed region, were providing favorable interaction with INH. This interaction helps INH to convert into its active form. However, in mutant enzyme, the interaction between binding residues and INH occurs at buried location and it resulted in the strong binding and hampered INH activation. It further provoked us to study the dynamics to understand the behavior of binding residues of enzyme. We investigated RMSF, RMSD, and *N*Hbond of wild and mutant enzyme in molecular dynamics simulation. Since the docking process is quite related to binding residues, we have highlighted RMSF of C-alpha carbon of binding residues with respect to time (Table 3).

In Fig. 3, Mutant *MtB*KatG showed less deviation till 30 ps from their starting structure, resulting in a backbone RMSD of ~0.11 nm and attained ~0.10 nm at 120 ps during the simulations, while wild structure showed a deviation of ~0.12 at first 30 ps and attained ~0.13 nm of backbone RMSD at 120 ps. Between a period of 200 to 500 ps, mutant structure showed frequent decrement (~0.14 to ~0.10 nm) in backbone C-alpha carbon RMSD, while wild exhibited opposite deviation and attained ~0.15 nm at 400 ps. A period of 500 to 670 ps showed that wild and mutant structure maintained similar deviation but after that wild gained RMSD dominant over mutant till 940 ps and attained RMSD of ~0.14 nm at 780 ps. After 940 ps till end, mutant showed more deviation than wild and attained ~12 nm at 945 ps. From the starting structures, mutant structure deviated less but wild exhibited more deviation. This magnitude of fluctuations together with the very small difference between the average RMSD values after the relaxation period (~0.11 nm) led to the conclusion that the simulations produced stable trajectories, thus providing a suitable basis for further analysis.

With the aim of determining whether the mutation affects the dynamic behavior of the residues, the RMSF


Fig. 5 Time evolution of hydrogen bonds among the main chain atoms of native and mutant structure. The symbol coding scheme is as follows: wild (solid lines) and mutant (dotted lines)

Fig. 6 Time evolution of number of distinct hydrogen bonds of 137D (**a**) , 230 V (**b**), 231 N (**c**), 232P (**d**) and 315 S/T (**e**) of wild and mutant to other amino acids within the enzyme during the simulations. The symbol coding scheme is as follows: wild (solid lines) and mutant (dotted lines)

values of the whole structure of wild and mutant *MtB*KatG were calculated, and are shown in Fig. 4. Analysis of the fluctuations revealed that more degree of flexibility was contained in wild than mutant enzyme. Moreover, the mutant also exhibited a decreased RMSF at the INH binding residues compared to wild enzyme (Table 3). Mean

error in flexibility was found as 0.01 for both C-alpha atoms in mutant and wild binding residues.

In Fig. 5, during first few picoseconds (~30 ps) mutant structure showed frequent increase in the hydrogen bonds (H-bonds) than wild structure. At 27 ps, mutant structure achieved highest number of hydrogen bonds of ~1152
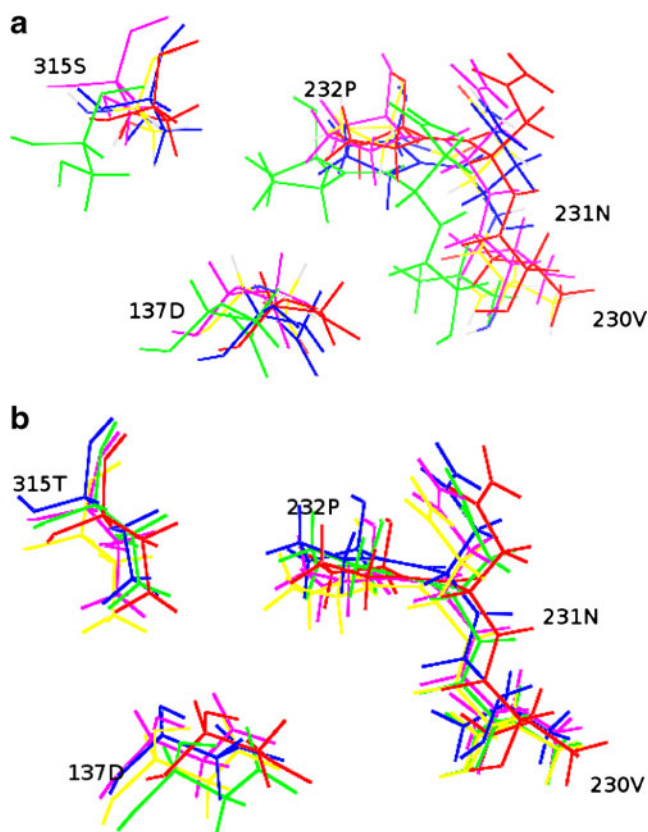
Fig. 7 Movement of INH binding residues (137D, 230 V, 231 N, 232P and 315 S/T) of wild (**a**) and mutant (**b**) enzyme during simulations. Average structures of INH binding residues at 0 to 200 ps (red), 200 to 400 ps (green), 400 to 600 ps (blue), 600 to 800 ps (magenta) and 800 to 1000 ps (yellow) has been superimposed

while, wild achieved ~1068 hydrogen bonds and loses ~84 hydrogen bonds compared to mutant structure. Between a period of 100-200 ps, both structures showed approximately similar number of H-bonds. Again between a period of 200-400 ps, wild loses ~30 H-bonds compared to mutant structure. The difference reaches ~100 H-bonds between a period of 400-480 ps. Between a period of 550-670 ps trajectories showed similar number of H-bonds in both mutant and wild but after this period again mutant dominated over wild by ~100 H-bonds till a period of 940 ps. At the end of the simulations (940-1000 ps) wild structure showed regain of~50 H-bonds compared to mutant structure. It is also evident from the plot (Fig. 5) that although the wild and mutant exhibited a different number of hydrogen bonds varies with time but it is steadily maintained throughout the simulations. *N*Hbond analysis further indicates the reason of rigidness of mutant structure as the increased number of H-bonds and more flexibility in wild structure due to less H-bonds, and is depicted in Figs. 4 and 5. There is also a significant observation between *N*Hbond analysis and RMSD analysis that wild enzyme exhibited more deviation (less deviation

in mutant enzyme) between a period of 200 to 480 ps and 650 to 900 (Fig. 3) and it was due to fewer H-bond formations between these periods (more H-bonds formation in mutant enzyme), it is shown in Fig. 5.

*N*Hbond analysis of 137D, 230 V, 231 N, 232P and 315 T of mutant has shown 0 to 2, 4 to 10, 1 to 4, 0 to 4 and 0 to 4 hydrogen bonds respectively, while in wild it has 0 to 2, 2 to 4, 1 to 2, 0 to 4 and 0 to 2 hydrogen bonds with surrounding residues respectively (Fig. 6). 230 V, 232P and 315 S/T have shown more degree of flexibility in wild and less in mutant enzyme (Table 3). The alteration in flexibility was validated by *N*Hbond analysis at INH binding residues. In wild enzyme, the binding residues exhibited more flexibility and have shown less participation in H-bonding with other amino acids, while mutant enzyme residues were rigid and have more H-bonds. On the basis of RMSF observation and *N*Hbond analysis, it is confirmed that the occurrence of the mutation leads to a less flexible or rigid INH binding site due to formation of more hydrogen bonds. Superimposed conformers of binding pocket of wild and mutant enzyme at different time scales during simulation were shown in Fig. 7a and b. It is clear that there are significant conformational changes in INH binding pocket. 230 N, 231 N, 232P and 315 S moves throughout the simulation in wild enzyme, while they showed less movement in mutant enzyme (Fig. 7a and b). 137D
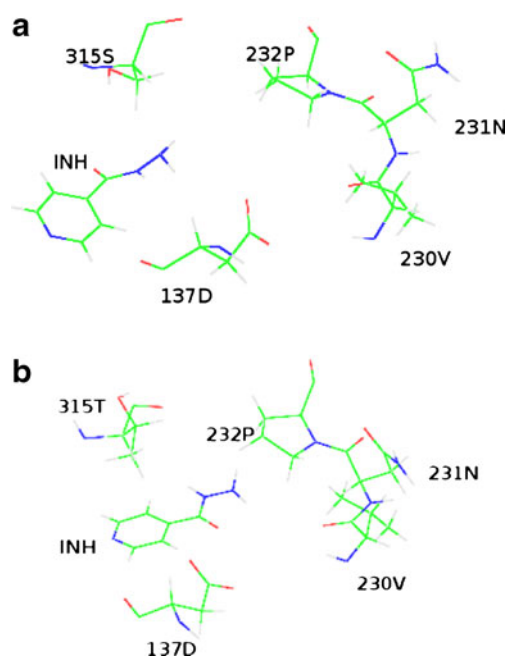
Fig. 8 (**a**) Binding mode of Isoniazid and *MtB*KatG wild type (**b**) Binding mode of Isoniazid and *MtB*KatG mutant type (S315T). The symbol coding scheme is as follows binding residues (137D, 230 V, 231 N, 232P and 315 S/T) and Isoniazid (INH) are shown in line model

exhibited a similar fashion of movement in both wild and mutant enzyme. The binding residues of wild enzyme showed significant fluctuations from starting structure (Fig. 7) during simulations and exhibited a considerable amount of structural flexibility (Table 3) due to lower involvement in H-bond formation with surrounding amino acids (Fig. 6). Analysis of these structures confirmed that the binding pocket of mutant enzyme has shown rigid or non-flexible pocket, while wild enzyme has a flexible binding pocket.

Our analysis strongly indicates that mutation (S315T) makes protein as well as the binding residues rigid and residues buried in 3D space. This behavior enables residues to exhibit strong electrostatic and van der Waals bonds with INH, while the flexible and exposed nature of binding residues of wild provide appropriate interaction with INH. This is also able to convert an active form of INH for inhibition activity. The binding mode of INH and binding residues of *MtB*KatG in 3D space shown in Fig. 8 a and b.

Conclusions

To gain insight into why the mutation (S315T) in *MtB*KatG confer INH resistance, docking, binding energetic analysis and short (~1000 ps) MD simulations in explicit solvent were performed on a mutant and wild catalase-peroxidase of *Mycobacterium tuberculosis*. Their structural fluctuations on a multi-picoseconds time scale were observed.

Wild structure exhibited a considerably low docking score of 2640, while mutant enzyme has displayed a high docking score of 2874. Mutant shown significant more affinity (binding energies of -7.53 kcal mol^{-1}) and exhibited less structural fluctuation at binding residues while wild structure shown more structural fluctuation and has less affinity (binding energies of -3.86 kcal mol^{-1}) toward INH. Moreover, mutation is able to decrease the conformational flexibility of the binding residues due to extra hydrogen bonding, as seen in molecular dynamics simulation. Variation within the H-bond networks affects intrinsic flexibility of the enzyme. Taken together, these data indicate that INH perform the best function when position 315th possess the serine residue and the mutation to threonine at the above position significantly impaired enzyme function, possibly by affecting the flexibility of the INH binding site and altering the 3D arrangement of binding residues. A real molecular understanding of mutation that renders *Mycobacterium tuberculosis* resistance to INH remains elusive. Our strategy enables scientists to study the diseases-causing by resistance bacterium in greater detail. Also it offers unprecedented insight into the interactions between the enzyme and the drug. The results are exposing promising new targets for drug therapy.

References

1. Zamocky M, Regelsberger G, Jakopitsch C, Obinger C (2001) The molecular peculiarities of catalase-peroxidases. FEBS Lett 492:177–182
2. Rouse DA, DeVito JA, Li Z, Byer H, Morris SL (1996) Site-directed mutagenesis of the katG gene of Mycobacterium tuberculosis: effects on catalase-peroxidase activities and isoniazid resistance. Mol Microbiol 22:583–592
3. Welinder KG (1991) Bacterial catalase-peroxidases are gene duplicated members of the plant peroxidase superfamily. Biochim Biophys Acta 1080:215–220
4. Nagy JM, Cass AE, Brown KA (1997) Purification and characterization of recombinant catalase-peroxidase, which confers isoniazid sensitivity in Mycobacterium tuberculosis. J Biol Chem 272:31265–31271
5. Zhang Y, Garbe T, Young D (1993) Transformation with katG restores isoniazid-sensitivity in Mycobacterium tuberculosis isolates resistant to a range of drug concentrations. Mol Microbiol 8:521–524
6. Singh AK, Kumar RP, Pandey N, Singh N, Sinha M, Bhushan A, Kaur P, Sharma S, Singh TP (2010) Mode of binding of the tuberculosis prodrug isoniazid to heme peroxidases: Binding studies and crystal structure of bovine lactoperoxidase with isoniazid at 2.7 A resolution. J Biol Chem 285:1569–1576
7. Wengenack NL, Rusnak F (2001) Evidence for isoniazid-dependent free radical generation catalyzed by Mycobacterium tuberculosis KatG and the isoniazid-resistant mutant KatG (S315T). Biochemistry 40:8990–8996
8. Timmins GS, Deretic V (2006) Mechanisms of action of isoniazid. Mol Microbiol 62:1220–1227
9. Johnsson K, King DS, Schultz PG (1995) Studies on the mechanism of action of isoniazid and ethionamide in the chemotherapy of tuberculosis. J Am Chem Soc 117:5009–5010
10. Hazbón MH, Brimacombe M, Bobadilla del Valle M, Cavatore M, Guerrero MI, Varma-Basil M, Billman-Jacobe H, Lavender C, Fyfe J, García-García L, León CI, Bose M, Chaves F, Murray M, Eisenach KD, Sifuentes-Osornio J, Cave MD, Ponce de León A, Alland D (2006) Population genetics study of isoniazid resistance mutations and evolution of multidrug-resistant Mycobacterium tuberculosis. Antimicrob Agents Chemother 50:2640–2649
11. Marttila HJ, Mäkinen J, Marjamäki M, Soini H (2009) Prospective evaluation of pyrosequencing for the rapid detection of isoniazid and rifampin resistance in clinical Mycobacterium tuberculosis isolates. Eur J Clin Microbiol Infect Dis 28:33–38
12. Dalla Costa ER, Ribeiro MO, Silva MS, Arnold LS, Rostirolla DC, Cafrune PI, Espinoza RC, Palaci M, Telles MA, Ritacco V, Suffys PN, Lopes ML, Campelo CL, Miranda SS, Kremer K, da Silva PE, Fonseca L de S, Ho JL, Kritski AL, Rossetti ML (2009) Correlations of mutations in katG, oxyR-ahpC and inhA genes and in vitro susceptibility in Mycobacterium tuberculosis clinical strains segregated by spoligotype families from tuberculosis prevalent countries in South America. BMC Microbiol 9:39
13. Ng VH, Cox JS, Sousa AO, MacMicking JD, McKinney JD (2004) Role of KatG catalase-peroxidase in mycobacterial

pathogenesis: Countering the phagocyte oxidative burst. Mol Microbiol 52:1291–1302

14. Marttila HJ, Soini H, Eerola E, Vyshnevskaya E, Vyshnevskiy BI, Otten TF, Vasilyef AV, Viljanen MK (1998) A Ser315Thr substitution KatG is predominant in genetically heterogeneous multidrug-resistant *Mycobacterium tuberculosis* isolates originating from the St. Petersburg area in Russia. Antimicrob Agents Chemother 42(9):2443–2445

15. Yu S, Girotto S, Lee C, Magliozzo RS (2003) Reduced affinity for Isoniazid in the S315T mutant of Mycobacterium tuberculosis KatG is a key factor in antibiotic resistance. J Biol Chem 278:14769–14775

16. Zhao X, Yu S, Ranguelova K, Suarez J, Metlitsky L, Schelvis JPM, Magliozzo RS (2009) Role of the oxyferrous heme intermediate and distal side adduct radical in the catalase activity of *mycobacterium tuberculosis* katg revealed by the w107f mutant. J Biol Chem 284:7030–7037

17. Ranguelova K, Suarez J, Metlitsky L, Yu S, Brejt SZ, Zhao L, Schelvis JP, Magliozzo RS (2008) Impact of distal side water and residue 315 on ligand binding to ferric Mycobacterium tuberculosis catalase-peroxidase (KatG). Biochemistry 47:12583–12592

18. Pym AS, Saint-Joanis B, Cole ST (2002) Effect of katG mutations on the virulence of Mycobacterium tuberculosis and the implication for transmission in humans. Infect Immun 70:4955–4960

19. Bertrand T, Eady NAJ, Jones JN, Jesmin NJM, Jamart-Gregoire B, Raven EL, Brown KA (2004) Crystal structure of Mycobacterium tuberculosis catalase-peroxidase. J Biol Chem 279:38991–38999

20. Heym B, Zhang Y, Poulet S, Young D, Cole ST (1993) Characterization of the katG gene encoding a catalase-peroxidase required for the isoniazid susceptibility of Mycobacterium tuberculosis. J Bacteriol 175:4255–4259

21. Zhao X, Yu H, Yu S, Wang F, Sacchettini JC, Magliozzo RS (2006) Hydrogen peroxide-mediated isoniazid activation catalyzed by Mycobacterium tuberculosis catalase-peroxidase (KatG) and its S315T mutant. Biochemistry 45:4131–4140

22. Berman HM, Westbrook J, Feng Z, Gilliland G, Bhat TN, Weissig H, Shindyalov IN, Bourne PE (2000) The protein data bank. Nucl Acids Res 28:235–242

23. Feldman J, Snyder KA, Ticoll A, Pintilie G, Hogue CW (2006) A complete small molecule dataset from the protein data bank. FEBS Lett 580:1649–1653

24. Schneidman-Duhovny D, Inbar Y, Nussinov R, Wolfson HJ (2005) PatchDock and SymmDock: servers for rigid and symmetric docking. Nucleic Acids Res 33:363–367

25. Han LY, Lin HH, Li ZR, Zheng CJ, Cao ZW, Xie B, Chen YZ (2006) PEARLS: program for energetic analysis of receptor-ligand system. J Chem Inf Model 46(1):445–450

26. Chothia C, Janin J (1975) Principles of protein-protein recognition. Nature 256:705–708

27. Fraczkiewicz R, Braun W (1998) Exact and Efficient Analytical Calculation of the Accessible Surface Areas and Their Gradients for Macromolecules. J Comput Chem 19:319–333

28. Shrake A, Rupley JA (1973) Environment and exposure to solvent of protein atoms. Lysozyme and Insulin. J Mol Biol 79:351–371

29. Rodriguez R, Chinea G, Lopez N, Pons T (1998) Vriend G. Homology modeling, model and software evaluation: three related resources. Bioinformatics 14(6):523–528

30. Hess B, Kutzner C, Spoel D, Lindahl E (2008) GROMACS 4: Algorithms for highly efficient, load-balanced, and scalable molecular simulation. J Chem Theory Comput 4:435–447

31. Spoel D, Lindahl E, Hess B, Groenhof G, Mark AE, Berendsen HJ (2005) GROMACS: fast, flexible, and free. J Comput Chem 26:1701–1718

32. Van Gunsteren WF, Billeter SR, Eising AA, Hunenberger PH, Kruger P, Mark AE, Scott WRP, Tironi TG (1996) Biomolecular simulation: The Gromos 96 Manual and User Guide. Hochschul-verlag AG an der Zurich, Zurich

33. Berendsen HJC, Postma JPM, van Gunsteren WF, Hermans J (1981) In: Pullman B (ed) Interaction models for water in relation to protein hydration. Intermolecular Forces. D Reidel Publishing Company, Dordrecht, pp 331–342

34. Berendsen HJC, Postma JP, van Gunsteren WF, DiNola A, Haak JR (1984) Molecular Dynamics with Coupling to an External bath. J Chem Phys 81:3684–3690

35. Essmann U, Perera L, Berkowitz ML, Darden T, Lee H, Pedersen LG (1995) A smooth particle mesh ewald method. J Chem Phys 103:8577–8593

36. Case DA, Pearlman DA, Caldwell JW, Wang J, Ross WS, Simmerling CL, Darden TA, Mertz KM, Stanton RV, Cheng AL, Vincent JJ, Crowley M, Tsue V, Gohlke H, Radmer R, Duan Y, Pitera J, Massova I, Seibel GL, Singh C, Weiner P, Kollman PA (2002) AMBER7 Simulation Software Package. University of California, San Francisco

37. Humphrey W, Dalke A, Schulten K (1996) VMD: visual molecular dynamics. J Mol Graph 14:33–38

38. Emsley P, Cowtan K (2004) Coot: Model-Building Tools for Molecular Graphics. Acta Crystallogr D - Biol Cryst 60:2126–2132